UNDERSTANDING THE PARAMETERS THAT INFLUENCE BUCKLING OF 3D FIBER-METAL LAMINATES

De Cicco, D., Taheri, F.*

Advanced Composite and Mechanics Laboratory, Department of Mechanical Engineering, Dalhousie University, 1360 Barrington Street, PO Box 15 000, Halifax, NS, B3H 4R2, Canada
* Corresponding author (farid.taheri@dal.ca)

Keywords: *buckling, finite element analysis, fiber-metal laminate*

ABSTRACT

In this paper, a simple numerical model was developed using LS-DYNA, a commercially available finite element software. The model was used to conduct a parametric study with the aim of investigating the performance of the 3D fiber-metal laminate (3D-FML) developed by our research group, under axial loading. The study evaluated effects of the initial perturbation, material properties, specimen's thickness, boundary conditions and gage length on the buckling response. The results produced by the study were validated by experimental results. The buckling capacity of the 3D-FML was also compared with respect to that of specimens made of aluminum and fiber-reinforced plastics, having equivalent bending stiffness. The intricacy in properly modeling the boundary conditions, and the sensitivity of buckling response to the way the actual boundary conditions are modeled numerically are also discussed.

1   INTRODUCTION

The use of fiber-reinforced polymer composites (FRP) in the automobile sector has been continually increasing. In fact, there is a global challenge in reducing the power consumption of vehicles with the aim to both lowering fuel consumption and reducing carbon emissions. Automotive companies have worked for decades on developing light-weight metallic alloys and fiber-reinforced plastic (FRP) for applications in transport vehicles, thereby to address the issue. One of the most effective means to reduce a vehicle's weight has been demonstrated to be attainable by taking advantage of marriage of light-weight metallic alloys and FRP. The outcome of such a marriage is referred to as fiber metal laminate (FML), consisting of an association of composite layers interleaved with thin metallic sheets. FMLs offer more superior attributes in terms of stiffness, strength, durability and resistance against impact, all with a significantly reduced weight compared to bulk metals or FRP counterparts.

A further improvement in energy absorption against out-of-plane impact of FMLs was demonstrated by our research group by means of using a new class of 3D fiber-glass fabric, instead of the conventionally used 2D fabric. Specifically, the 3D fabric, whose core cavities are filled by a foam, is sandwiched between light-weight magnesium sheets [1]–[4]. This combination results in an exemplary light-weight and resilient 3D fiber-metal laminate (3D-FML). While the performance of this 3D-FML for application in transport vehicle auto-body components has been extensively investigated under both static and dynamic loading by our group, its performance under an axially applied load has not been explored. Therefore, to address safety of vehicles, which is the most critical design constraint, the performance of this hybrid composite material under axial compressive loading must be systematically investigated. Several studies on the response of FRP under axial load (i.e., buckling) are available in the literature, with a few which have investigated the buckling of sandwich and FML composites. For instance, Remmers and de Borst [5] studied effect of buckling delamination in Glare-FML, under quasi-static compressive force by numerical simulations. They modeled each layer of the aluminum and FRP with solid-like shell elements, interleaved with interface elements to account for delamination. Hwang and Liu [6] conducted experimental studies on both buckling and post-buckling

response of laminated composites hosting multiple delaminations. They highlighted the different buckling modes with respect of delamination position in the stacking sequence. They also showed that the specimens could carry load after reaching their buckling stage. Also, Kollár [7] developed a series of simple analytical equations for predicting the buckling of thin walled FRP beams of various cross sections. The validity of their analytical results was corroborated with finite element simulations.

Focusing more on sandwich structures, Frostig [8] developed a higher-order theory to predict the buckling behavior of sandwich panels having a flexible core. The analytical predictions were validated with numerical results. Gdutos et al. [9] studied the face wrinkling failure of aluminum-honeycomb sandwich columns under various loading conditions. They concluded that wrinkling of the faces was more likely to occur in specimens with long spans. They also observed that delamination of the faces was another phenomenon that could likely occur. Similarly, Vonach and Rammerstorfer [10] examined the wrinkling of thick orthotropic plates subjected to general loading conditions, both analytically and numerically. The numerical results were in accordance with the analytical ones.

To the best of authors' knowledge, works specifically exploring buckling of 3D-fiber metal laminates are limited to [1]–[4], in which it has been demonstrated that several factors affect the response. Therefore, understanding the influence of various parameters that govern the stability of this 3D-FML under in-plane loading is of paramount importance, enabling one to optimize the performance of the material when used in vehicles. It should be noted that experimental examination of the parameters that influence the stability response of such composites would not be a feasible approach. Therefore, the objective of this research is to conduct a numerical investigation with the aim of better understanding the influence of some of the parameters that significantly affect the stability of the 3D-FML. Finite element analysis (FEA) is considered to be one of the most effective and efficient means to conduct parametric studies [11]–[13]. In our preliminary investigation, we consider a relatively simple, yet relatively accurate and efficient numerical model, developed in LS-DYNA environment FEA software. MATLAB was used to facilitate the process of permutations of the considered parameters. Experimental results were used to validate the numerical predictions, rendering the simplified approach to be adequately effective and accurate. More experimental investigations will be carried out in the next phase of the study to further validate some of the FEA results.

2   NUMERICAL PROCEDURE

2.1   Modeling approach

Numerical simulations of the buckling response of the 3D-FML under static axial compressive load were performed using LS-DYNA, a commercial finite element (FE) software. An experimental investigation was also conducted to validate the numerical results. A simplified approach was used to model the entire 3D-FML (i.e., all its constituents) using a single layer of shell elements (cf. Figure 1). The model, however, accounted for each of the constituents (i.e., the magnesium alloy skin, fiberglass plies and the combined glass pillars/foam core region), using their respective material properties and thickness, inputted via the keyword *PART_COMPOSITE. In this way, a separate integration point is attributed to each material constituent. Note that all layers are assumed to be tied together, thus inhibiting modeling of any potential delamination. Table 1 presents a summary of the FE model.

The magnesium alloy skins were modeled using the plasticity model *MAT_PIECEWISE_LINEAR_PLASTICITY, and the fiberglass plies were modeled using *MAT_ENHANCED_COMPOSITE_DAMAGE, which is an orthotropic material model, with Chang-Chang damage criterion, recommended for modeling fiber-reinforced composites. Response of the combined glass pillars/foam of the core was modeled using the plasticity model *MAT_LAYERED_LINEAR_PLASTICITY. A better choice for modelling would be the use of crushable foam model; however, this model cannot be used in conjunction with the shell element in LS-DYNA. Therefore, the actual stress-strain curve of the foam was in the model. Also, the implicit solver, with the arc-length method enabled, was used to obtain the post buckling behavior.

Furthermore, Kenny [14] demonstrated the need for modelling the actual restraining text fixture for obtaining accurate buckling behavior. In our analyses, however, the fixtures themselves were not modeled, but their effect on the end portions (22 mm at each end) of the specimens was taken into account by applying the appropriate boundary conditions over the segments that were actually restrained (gripped) by the test fixture.

The use of a perturbation (or incorporation of small imperfection) in the mesh, is a common procedure in order to initiate the buckling process. Here, the specimen imperfection was modeled by perturbing the mesh in the lateral direction by:

$$p(x) = A \sin \frac{\pi x}{L_{tot}}$$
(1)

where $p(x)$ is magnitude of the lateral imperfection, A is the amplitude of the maximum imperfection, and L_{tot} is the total length of the specimen (including the parts held in the fixture). This imperfection was selected based on the actual imperfections extracted from the images recorded during the experimental tests; this also conforms to the natural curvature seen in most auto body components.

The material properties were obtained from in-situ tests. The modulus of elasticity and tensile strength of the 3D fiberglass fabric resulted to be substantially lower than its equivalent unidirectional counterparts, mainly due to the knitting process and the actual high resin content pockets. Note that, as seen in Figure 1, the in-plane axial load was applied at one of the extremities of the specimen.

Figure 2 illustrates the deformed shape obtained numerically, superimposed on the actual deformed shape of a typical specimen, at a load prior to onset of buckling. As can be seen, the two shapes match precisely. However, the agreement holds up to the load prior to the load at which delamination buckling occurs in the specimens. As clearly visible from the load-axial shortening curve in Figure 3, the specimen buckles and the load capacity drops drastically once an axial shortening of around 1.5 mm is attained. The failure mechanism involves delamination of the magnesium skin from the fiberglass ply, on the surface that undergoes compression (cf. Figure 2 (b)). As mentioned previously, since the numerical model cannot simulate any delamination, the numerical results cannot be compared against experimental results after the onset of delamination. Moreover, the good agreement between the numerical and experimental results seen in Figure 3 attests to the adequacy of this relatively simple model in capturing the instability response of this complex system in a fairly accurate manner, thus rendering the model adequate for the subsequent parametric studies. This model is, therefore, used to investigate the influence of various parameters on the stability response of the FML. The parameters that would be considered are the imperfection amplitude, component's thicknesses, material properties, as well as various boundary conditions and gage lengths. A MATLAB code was developed by which the necessary variation in the parameters used in LS-DYNA's input file could be generated and run automatically in the runs that did not require construction of a new FE mesh, thus increasing the efficacy of the numerical analyses.

To facilitate readers' understanding of the parametric study, a summary of the parameters that were used in the study is provided in Table 2. The following abbreviations are used in this study; Mg: magnesium; Al: aluminum; Fg: fiberglass; Cf: carbon-fiber; Fo: the foam used in construction of actual specimens; Fw and Fs refer to the foams with a lower and higher density than that used in actual specimens, respectively, and Fix and Pin refer to fixed and pinned boundary conditions, respectively.

Constituent	No. integration points	Thickness (mm)	Material model
Top skin	1	0.5	*MAT_024
Top ply	1	0.45	*MAT_054
Core	2	3.4 (1.7 at each point)	*MAT_114
Bottom ply	1	0.45	*MAT_054
Bottom skin	1	0.5	*MAT_024

Table 1: Specifics of the FE model.

Parameter whose effect is considered	Perturb. Amplitude (mm)	Thickness			Material type			Length		B.C.
		Skin thickness (mm)	Ply thickness (mm)	Core thickness (mm)	Skin	Ply	Core	Gage length (mm)	Length of restrained portion (mm)	
Imperfection	0, 0.05, 0.1, 0.2, 0.5, 1, 1.5, 2, 5	0.5	0.45	3.4	Mg	Fg	Fo	150	22	Fix-Fix
Thickness	1	0.5, 0.8, 1	0.45, 0.6, 1	1.4, 3.4	Mg	Fg	Fo	"	"	"
Properties	"	0.5	0.45	3.4	Mg, Al	Fg, Cf	Fo, Fw, Fs	"	"	"
B.C.	0.05	"	"	"	Mg	Fg	Fo	150	22 or none	Fix-Fix, Fix-Pin, Pin-Pin, Fix-Free
Length	"	"	"	"	"	"	"	150, 175, 200, 225, 250, 300	22	Fix-Fix

Table 2: Summary of the parameters used in the numerical studies.

Figure 1: The FE mesh, boundary conditions and applied load.

(a)

(b)
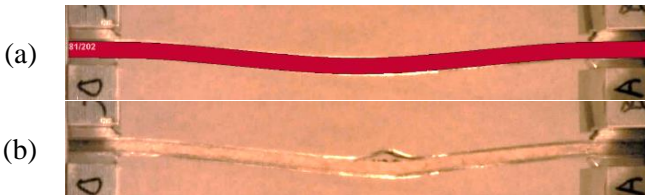
Figure 2: Comparison of the experimental and numerical deformed shapes; (a) FE model superimposed in red on an actual deformed specimen, (b) Actual mode of failure due to delamination of the skin.
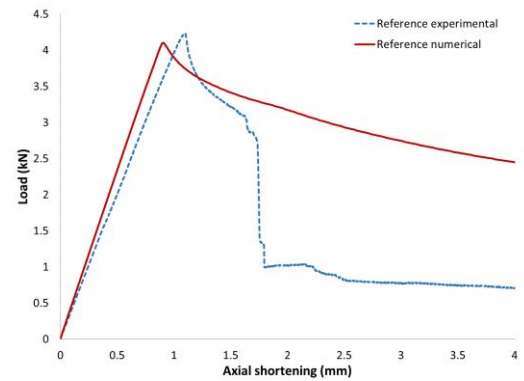
Figure 3: Comparison of experimental and numerical results for the reference specimen.

2.2 Effect of Mesh Density

A mesh convergence study was carried out to establish the most appropriate mesh density by which consistent and fairly accurate results could be obtained, with minimal CPU consumption. For consistency, all models were run on a single core. Figure 4 shows that convergent results are achieved with a mesh of 6x97 elements. It can be noted that increasing the number of elements in the width direction from six to ten did not improve the computed results, but it did not increase the CPU time, either. Therefore, the chosen mesh density for all simulations presented in this paper has been taken as 10x97. It should be noted the same mesh density was scaled and used in modelling longer specimens. In addition to the mesh convergence study, the effect of the number of integration points for modeling the foam, whose thickness is relatively much greater than thickness of the other constituents, was also investigated. Two

simulations, one with two integration points, and another one with 20, were considered. No significant difference in the results was noted; therefore, the subsequent analyses were carried out with two integration points for the foam.
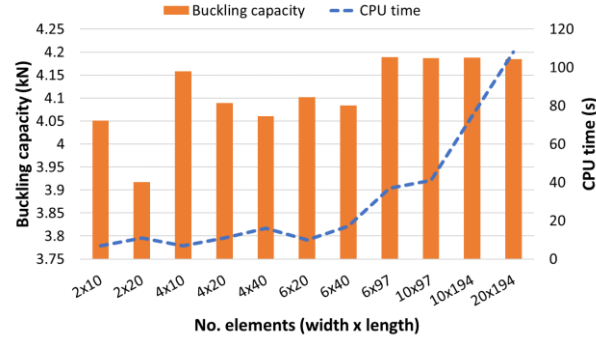
Figure 4: Results of the mesh convergence study.

3   RESULTS AND ANALYSIS

3.1   *Effect of Imperfection Amplitude*

As described by equation (1), the imperfection was assumed to be in a half-sine wave shape with an initial amplitude of 1 mm; however, amplitudes ranging from 0 to 5 mm were tested and their effect on the behavior is reported in Figure 5 and Figure 6. As can be seen, the specimen with 5 mm amplitude exhibited a response that could not be considered as a buckling response; therefore, it was not be taken into account, thus not reported in Figure 6.

From Figure 5, it is clear that the imperfection has negligible influence on the stable or pre-buckle response of the specimen, while it clearly influences the buckling load and post buckling response of the specimens. For the lower imperfection values, the "snap-bulking" phenomenon is noticeable. The significant decrease in the buckling capacity becomes more evidence for specimen with 0.05 mm and greater imperfections. The specimen with 1 mm imperfection exhibits 20% loss in buckling capacity compared to the one with the lowest imperfection. Also, it worth noting that buckling is observed in the specimen with no initial imperfection. The numerical uncertainties appear to be triggering the instability.
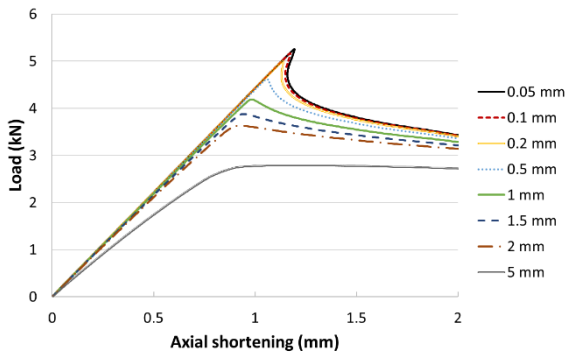
Figure 5: Load-axial shortening curves of models having different imperfection amplitudes.
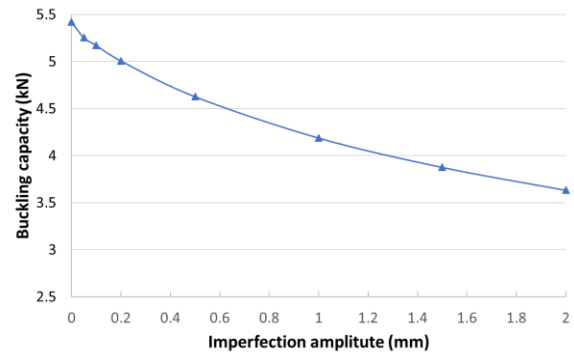
Figure 6: Variation of the buckling capacity as a function of imperfection amplitudes.

3.2   Effect of Constituents' Thickness

In this section the effect of constituents' thickness on buckling response is investigated. The variations in the thicknesses as reported in Table 2 was selected based on the actual commercially available dimensions. The first aspect of the change in behavior is observable in Figure 7, where the thickness of the core seems to greatly influence the pre-buckling or stable response of the specimens. In fact, in the case of 3.4 mm thick core, the response is linear, while it becomes nonlinear when thinner cores are considered. Also, the axial shortening at which the buckling occurs is relatively lower when a thinner core is used. On the contrary, the post-buckling behavior seems to be influenced by the FRP plies' thickness; in fact, after the onset of buckling, the specimens with thicker FRP plies tend to carry more load than those with relatively thinner plies. Finally, as expected, the metallic skin thickness seems to have comparatively the greatest impact on the buckling capacity than the other constituents. This is because the skins, which are the outer parts of the system, encounter the greatest stress; therefore, since they are the stiffest constituent, they influence the buckling capacity significantly.

The other interesting behaviour can be seen from the results illustrated in Figure 8, which presents the buckling capacity as a function of the normalized flexural stiffness. The results are normalized in three different ways. First, the results are normalized with respect to the weight of the 3D-FML with x.x foam thickness (referred to as 3D-FML – x.x mm foam). The second set of results are normalized with respect to the weight of an aluminum specimen having equivalent bending stiffness as that of the 3DFML with x.x thickness (i.e., Al.– x.x mm foam). Finally, the third set is normalized with respect to the weight of a fiber-glass/epoxy specimen, having the same bending stiffness as 3D-FML specimens with x.x foam thickness (i.e., FRP – x.x mm foam). The equivalent aluminum and FRP specimens have the same width and length as the 3D-FML. In addition, the stacking sequence of the FRP specimens were limited to biaxial fiber-orientations, with a symmetric configuration. The following configurations were considered: $[(0/90)_n / \overline{0}]_s$, $[(0/90)_n / 0]_s$, $[(0/90)_n / 0/\overline{90}]_s$, and $[(0/90)_n]_s$. The normalization is done based on the following equation:

$$Normlization = \frac{D_{11}^i}{W_i} \tag{2}$$

where D_{11} is the axial bending stiffness, W is the weight of 3D-FML specimen or the specimen with equivalent stiffness, and i is the specimen configuration identifier.

The normalized results illustrated in Figure 8 highlight the superior buckling capacity offered by the 3D-FML from the perspective of weight. One can see that the 3D-FML is clearly the most efficient configuration, followed, in order of performances, by the FRP and aluminum. A distinction between the cases, whose results were normalized with respect to the overall thicknesses, is also discernable. The buckling capacity suffers as the thickness becomes smaller, regardless of the material and configuration.

It is necessary to mention that in real applications, the above-mentioned superior buckling capacity of the 3D-FML might become affected by the onset of skin/FRP-ply interface delamination. In fact, as highlighted in previous works [3], [4], delamination-buckling of one of the skins could occur at a load lower than the theoretically-established buckling capacity. As stated previously, the relatively simple model used here does not account for such a delamination mechanism. However, one can confidently conclude that an improvement in the interface bond strength should enable the specimens to attain their theoretical buckling capacity.
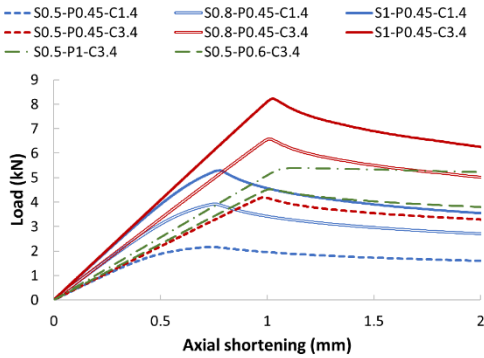
Figure 7: Load-axial shortening curves for different component thicknesses.
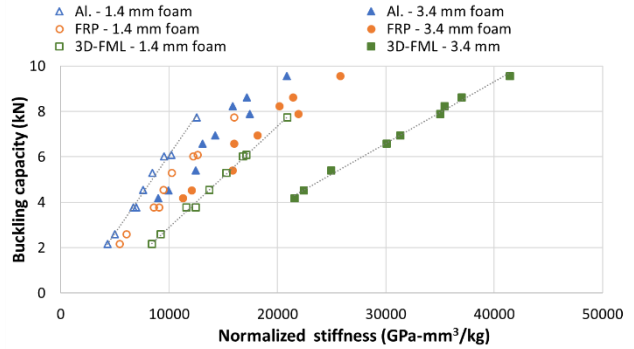
Figure 8: Buckling capacity versus normalized bending stiffness.

3.3   Material properties

Another focus of the study was to investigate the influence of material properties on the buckling response. For that, a different material was considered to form the skin. Aluminum 2024-T3 was selected in this part of the investigation due to its light-weight, and extensive use in various applications, especially its usage in the aerospace sector. The properties of this aluminum was extracted from [15]. Another permutation was achieved by replacing the 3D fiberglass fabric with an equivalent carbon-fiber fabric, whose properties were obtained through our previous mechanical tests conducted on a unidirectional carbon fabric. Finally, the stress-strain curve of the foams having lower and higher density than the one used in the actual specimens were estimated based on the supplier's information and the actual properties of the reference foam, obtained experimentally. Therefore, the lower density foam's stress-strain curve was established by degrading (scaling down) the reference foam's stress-strain curve by 33%, while the higher-density foam's stress-strain curve was scaled up by 2.5 times.

The resulting buckling capacities are summarized in Figure 9, and are reported with respect to the normalized stiffness, according to the same normalization procedure explained in previous section. As seen, similar pattern in behavior is observed, with the best performance exhibited by the 3D-FML, followed by FRP and aluminum, respectively. Moreover, results illustrated in Figure 9 and Figure 10 reveal that a gain of 50% in the buckling capacity can be attained by replacing the magnesium skins with aluminum. This is combined with a 24% decrease in the axial shortening prior to buckling. Note that the results corresponding to the foam properties are not reported, because they did not have a significant influence on buckling response of the 3D-FML within the considered range.

The effect of carbon fabric is reported in Figure 9 as well. The same pattern as observed for the case of glass fabric is visible. In addition, interestingly, an overall increase of 0.8 kN in the buckling capacity is observed for all skin-foam configurations (e.g., increase from 4.2 kN to 5 kN and increase from 6 kN to 6.8 kN, as seen in Figure 9), which represents a 22% increase in the case where magnesium skins are used. Furthermore, the load-axial shortening curves of the four materials combinations are illustrated in Figure 10. The results indicate that properties of the skins have the most influence on buckling response, while the maximum buckling capacity is both affected by properties of the skins and FRP plies.
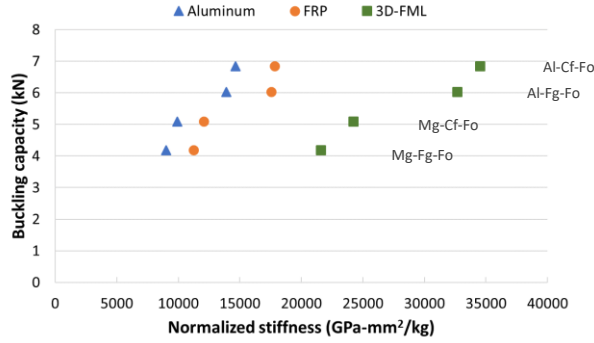
Figure 9: Buckling capacity versus normalized bending stiffness, for different material properties.
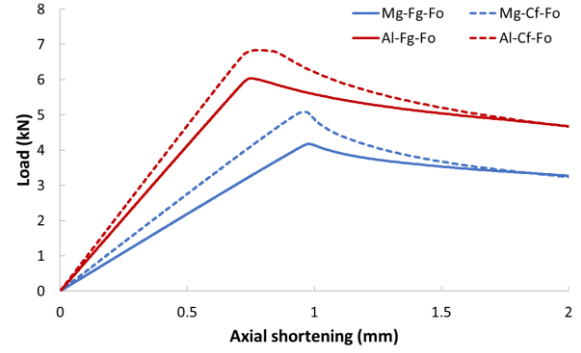
Figure 10: Influence of the material properties on buckling response.

3.4   *Influence of Boundary conditions*

It is well known that boundary conditions (BCs) have a significant influence on the buckling capacity of axially loaded members. For this reason, the four most commonly used BCs, namely: fixed-fixed, fixed-pinned, pinned-pinned and fixed-free, are simulated and the resulting buckling capacities are compared. The comparison is made purely from a numerical point of view; the comparison with experimental results will be the focus of our future works. For all the tests, the gage length is kept constant at 150 mm and the amplitude of the imperfection is reduced to 0.05 mm to promote a distinct buckling behavior under all conditions.

The results are presented in Figure 11. As expected, the fixed-fixed setup offers the highest buckling resistance capacity, follow by the fixed-pinned specimen with 27% reduction, pinned-pinned with 62% and fixed-free, with 91% reduction in buckling capacity. Furthermore, the critical buckling load of a composite column can be estimated with the Euler buckling equation, and the use of an appropriate factor provided to account for the boundary conditions, as follows:

$$P_{cr} = \frac{\pi^2 b D_{11}}{(kL)^2}$$

with:
$k = 0.5$ for fixed-fixed
$k \approx 0.7$ for fixed-pinned
$k = 1$ for pinned-pinned
$k = 2$ for fixed-free

(3)

In above equation, P_{cr} is the buckling capacity, L and b are the gage length and width of the specimen. Equation (3) predicts a quadratic variation of the critical buckling load with respect to the BCs. However, the result obtained from the simulations, as illustrated in Figure 11, reveal a linear variation.

In order to establish whether the cause of observed disagreement could be due to an incorrect modeling approach, the buckling response of the same specimen (i.e., the same FE model), but this time made of single isotropic material (i.e., the magnesium alloy) was considered. The results, also reported in Figure 11, show the same linear pattern as observed for the 3D-FML case. This would indicate that the way the boundary conditions have been modeled is causing the discrepancy. Note that a more appropriate modelling of the BCs would necessitate the use of a 3D FE model.
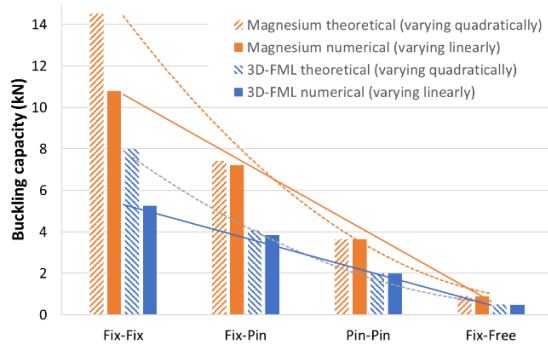
Figure 11: Buckling load for different boundary conditions.
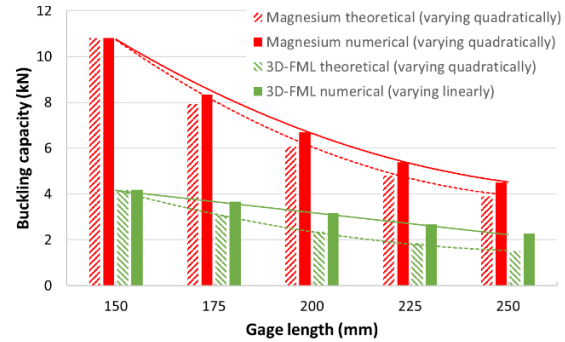
Figure 12: Buckling load for various gage lengths.

3.5   *Influence of the Gage length*

The last influencing aspect investigated in this work is the effect of gage length on the buckling load capacity of the 3D-FML. Fixed-fixed boundary conditions were used and the imperfection amplitude was varied in such a way that the same curvature could be obtained for all selected lengths. In fact, as mentioned in [16], keeping the same perturbation amplitude for all specimen lengths led to more consistent results.

The results of the analyses are reported in Figure 12. As expected, the buckling load decreases when the gage length increases. However, equation (3) indicates that the variation should follow a quadratic trend, while the numerical results show a linear trend. Once again, isotropic simulation was used to pinpoint the source of the discrepancy. The obtained results, also reported in Figure 12, show that, in the case of isotropic material, the variation follows the expected quadratic trend. This would suggest that in the case of 3D-FMLs, additional coupling effects exist that would need to be taken into consideration. Perhaps resolution of this parameter would also resolve the trend discrepancy observed and discussed in last section.

4   CONCLUSION

A numerical model of the newly developed 3D-FML was constructed using the finite element software LS-DYNA. Parametric studies were carried out to investigate the influence of various parameters on the buckling response of the FML, highlighting the most influencing factors. The influence of imperfection amplitude, constituents' thickness and properties, boundary conditions, and gage length were considered.

The results of the investigation can be summarized as follows:

- The initial perturbation or imperfection influences the buckling capacity and post-buckling behavior of the 3DFMLs, but its effect on the pre-buckled regime is insignificant.
- The core (or foam) thickness is the parameter that most influences the buckling capacity. This is also the parameter that enables the 3D-FML to outperform the stability response of specimens made of either aluminum or FRP possessing the same stiffness.
- The skins properties have important influence on the buckling capacity. For the majority of practical core thicknesses, the stiffer the skins, the more linear would be the pre-buckling behavior.
- The boundary conditions and the way they are conventionally modeled numerically affect the predicted results significantly. The numerical results did not follow the trend predicted by the Euler equation, when either isotropic or orthotropic material was considered. This highlights the fact that when modelling thick and relatively short geometries, the use of conventionally applied FE boundary conditions would not produce accurate results, and that the actual restraining mechanism must be carefully and meticulously modeled.

- Similar to the effect of BCs, it was demonstrated that the variation of buckling load with respect to the gage length did not follow the Euler prediction in the case of the 3D-FML, while it did follow the Euler prediction when the material was isotropic. This nonconformity could be as the outcome of inadequate modeling of BCs associated with the use of 2D FE modelling approach. The perturbation mode could also influence the effect of this parameter.

In closing, it is necessary to mention that the incapability of the rather simple modelling approach used in this study, in detecting delamination, limits the use of the model. This incapability results in gross over-prediction of the post-buckling load-carrying capacity. Our experimental investigation also demonstrated that in shorter specimens that would not buckle, the failure mode is associated with total debonding of the skin from FRP. This mechanism could not be detected by the simplified modelling approach either. However, the simplified modelling approach could be effectively used to investigate the influence of various parameters that could affect the buckling response of the 3D-FMLs. Moreover, the model clearly shows that improved buckling and post-buckling performances could be obtained by improving the bond strength of skin/FRP interface. In all, the very efficient computation CPU-time associated with the use of this simplified modelling approach warrants its use for preliminary parametric investigations.

5 REFERENCES

[1] Z. Asaee, S. Shadlou, and F. Taheri, "Low-velocity impact response of fiberglass/magnesium FMLs with a new 3D fiberglass fabric," *Compos. Struct.*, vol. 122, pp. 155–165, 2015.

[2] Z. Asaee and F. Taheri, "Experimental and numerical investigation into the influence of stacking sequence on the low-velocity impact response of new 3D FMLs," *Compos. Struct.*, vol. 140, pp. 136–146, 2016.

[3] D. De Cicco and F. Taheri, "Delamination Buckling Response of 3D Fiber-Metal Laminates Subjected to Different Loading Rates," in *Proceedings of the American Society for Composites: Thirty-First Technical Conference*, 2016, p. 12.

[4] Z. Asaee, M. Mohamed, S. Soumik, and F. Taheri, "Experimental and numerical characterization of delamination buckling behavior of a new class of GNP-reinforced 3D fiber-metal laminates," *Thin-Walled Struct.*, vol. 112, no. December 2016, pp. 208–216, 2017.

[5] J. J. C. Remmers and R. de Borst, "Delamination buckling of fibre-metal laminates," *Compos. Sci. Technol.*, vol. 61, no. 15, pp. 2207–2213, 2001.

[6] S.-F. Hwang and G.-H. Liu, "Experimental Study for Buckling and Postbuckling Behaviors of Composite Laminates with Multiple Delaminations," *J. Reinf. Plast. Compos.*, vol. 21, no. 4, pp. 333–349, 2002.

[7] L. Kollár, "Local buckling of fiber reinforced plastic composite structural members with open and closed cross sections," *J. Struct. Eng.*, vol. 129, no. 11, pp. 1503–1513, 2003.

[8] Y. Frostig, "Buckling of sandwich panels with a flexible core—high-order theory," *Int. J. Solids Struct.*, vol. 35, no. 97, pp. 183–204, 1998.

[9] E. . Gdoutos, I. . Daniel, and K.-A. Wang, "Compression facing wrinkling of composite sandwich structures," *Mech. Mater.*, vol. 35, no. 3–6, pp. 511–522, 2003.

[10] W. K. Vonach and F. G. Rammerstorfer, "Wrinkling of thick orthotropic sandwich plates under general loading conditions," *Appl. Mech.*, vol. 70, no. January 1999, pp. 338–348, 2000.

[11] E. Fuoss, P. V. Straznicky, and C. Poon, "Effects of stacking sequence on the impact resistance in composite laminates. Part 2: prediction method," *Compos. Struct.*, vol. 41, no. 2, pp. 177–186, 1998.

[12] F. Fu, D. Lam, and J. Ye, "Parametric study of semi-rigid composite connections with 3-D finite element approach," *Eng. Struct.*, vol. 29, no. 6, pp. 888–898, 2007.

[13] P. B. Stickler and M. Ramulu, "Parametric analyses of stitched composite T-joints by the finite element method," *Mater. Des.*, vol. 23, no. 8, pp. 751–758, 2002.

[14] S. Kenny, "Dynamic Pulse Buckling of Slender Beams with Geometric Imperfections Subjected to an Axial Impact," Dalhousie, 2001.

[15] Varmint's Al, "Varmint's Al's Engineering Page." [Online]. Available: http://www.varmintal.com/aengr.htm.

[16] Z. Zhang and F. Taheri, "Dynamic Pulsebuckling Analysis of FRP Composite Laminated Beams Using LS-DYNA," *7th Int. LS-DYNA Users Conf.*, no. 1, pp. 41–48.